Electrochemical behavior of thick rust layers on steel artefact: Mechanism of corrosion inhibition

Emmanuel Rocca, Hadri Faiz, Philippe Dillmann, Delphine D. Neff, François Mirambet

Electrochemical behavior of thick rust layers on steel artefact: mechanism of corrosion inhibition

Emmanuel Rocca, Hadri Faiz, Philippe Dillmann, Delphine Neff, François Mirambet

1. Institut Jean Lamour, Université de Lorraine, Dept CP2S,

BP 50840 - Campus Artem, 2 allée André Guinier, 54011 Nancy cedex - France

2 IRAMIS/LAPA - CEA Saclay –91911 Gif-sur-Yvette, France

3. C2RMF, Centre de recherche et de restauration des musées de France, Palais du Louvre - Porte des Lions 14 Quai François Mitterrand, 75001 Paris, France

Abstract

The electrochemical behavior of aged corrosion layers (CL) on artefact was studied, in corrosive reference water without and with non-toxic corrosion inhibitors such as decanoate ions and flavonoids compounds, constituting the condensed tannins, such as catechin. Electrochemical impedance spectroscopy measurements on the metal/CL system and voltammetric studies of FeOOH phases on carbon paste electrode show that the corrosion inhibition mechanism is mainly based on the blocking of the dissolution of FeOOH-type phase and the decrease of the diffusion of ionic species in the pores network of CL. Indeed, the formation of iron decanoate, revealed by X-ray diffraction and microscopic observation, inhibits the electrochemical activity of FeOOH-type phases and blocks the electrochemical dissolution of FeOOH into Fe^{2+} cations. On the other hand, the catechin compound modifies the surface of rust compounds into a blue-black compound, but this modification has a poor influence on the electrochemical activity of FeOOH-type compounds.

Keywords: corrosion layer, corrosion inhibition, FeOOH, impedance spectroscopy, carbon paste electrode

1. Introduction

Since the middle of the 20th century, an increasing number of materials, objects of the industrial heritage are preserved in heritage institutions. Their preservation is of great importance considering their historical, technological, architectural and scientific values. This heritage consists of buildings and machinery, workshops, mills and factories, mines and sites for processing and refining… [1]. Among the objects conserved in museum collections, a significant part are covered by thick rust layers, especially items in cast iron or steel from the industrial revolution in the last half of the 18th century. These corrosion layers (CL) should be preserved because they also contain some traces of manufacturing and use of the objects. Moreover, the important size of many industrial artefacts needs to expose or to store them outside or in sheltered conditions without control of the environmental parameters.

In cyclic atmospheric conditions, Evans and Taylor [2] have first proposed a cyclic electrochemical mechanism to explain the formation of thick rust layers on iron substrate in atmospheric conditions. This cyclic mechanism can be described as follows. During a first wetting step, the iron(III) oxyhydroxides (FeOOH) are progressively dissolved into iron(III) cations which oxidize the iron metal into iron(II) compounds throughout the pores of the corrosion layer. Then, once the metal is covered by a thick water layer, the iron metal is mainly oxidized by dissolved oxygen into iron(II) compounds. Next, the drying step induces a progressive decrease of water thickness on surface and a rapid diffusion of oxygen gas across the thin water layer leading to both the oxidation of iron(II) species into iron(III) oxyhydroxide and the oxidation of iron into Fe(II).

This mechanism, experimentally demonstrated by M. Stratman et al. [3, 4], is mainly controlled by the dissolution-precipitation process of different iron(II) and iron(III) solid compounds during wet-dry cycles. During this cycle, the oxygen access inside the CL has been underlined as an important parameter by several authors [5]. Moreover, the electronic

conductivity of each iron oxide phase and their connectivity with the iron substrate are important parameters defining the localization of the oxygen reduction, but don't modify the overall Stratman's mechanism [6-9]. In fact, ancient corrosion layer are often characterized by a complex mixing of several oxyhydroxide phases with different stratification, mainly depending on atmospheric conditions along their ageing [10].

Only few studies propose a comprehensive electrochemical characterization of the phenomenon occurring inside a thick CL on steel [11-14]. From impedance measurements on corroded cast iron pipe, I. Frateur et al. have first proposed a description of the electrochemical phenomenon of cast iron in presence of CL [11, 12] based on de Levie's conductive porous electrode model [13], in immersed conditions in water electrolyte. This electrochemical model was confirmed and adapted in the case of corroded cast iron in water pipe [14].

For cultural heritage, the cleaning of corroded surface can be required by curators to homogenize the surface aspect and to avoid the formation of red pits on surface during exposure in uncontrolled atmospheres [15, 16]. Nowadays, different treatments are implemented by conservators such as conversion treatments with polyphenol macromolecules based on flavonoids groups, named tannins [17, 18], or with more aggressive phosphating solutions [19]. Unfortunately, these treatments can induce important modifications of the color aspect. The use of varnish or paints is also an interesting method of protection for objects exposed in outdoor in unsheltered conditions, but the change of aspect can be drastic in this case. Now, the conservation of the corrosion layers without modifications of aspect requires the development of specific treatments. Moreover, the important size of these objects requires that the treatment is realized on site with non-toxic and easy process.

In this framework, the present work aims to study the effect of non-toxic corrosion inhibitors as carboxylate and flavonoid compounds on the electrochemical behavior of aged corrosion

layers on steel. In fact, sodium carboxylate or carboxylic acid have been already investigated as corrosion inhibitors on many metals such as zinc, copper, steel, magnesium alloys or lead [20-24]. And catechin is the main flavonoid species, which constitutes the monomer of condensed tannin [25].

The objective is to investigate the corrosion inhibition mechanism by studying, both the electrochemical behavior of the metal/CL system with or without corrosion inhibitor, and the influence of corrosion inhibitor on the electrochemical activity of different iron(III) oxyhydroyde phase of CL by the carbon paste electrode (CPE) technique.

Firstly, the metal/CL system was studied by electrochemical impedance spectroscopy (EIS) in corrosive water with or without inhibitor. Then, a corrosion inhibition treatment of the metal/CL system is proposed and was characterized by EIS in corrosive conditions. The corrosion layer and iron(III) oxyhydroxide treated and non-treated by corrosion inhibitors were characterized by Raman spectroscopy, X-ray diffraction (XRD) and scanning electron microscopy (SEM) coupled with energy dispersive X-ray spectroscopy (EDX).

2. Experimental

The corroded steel samples, provided by the Musée Les Mineurs Wendel in the ancient site of a coal mine at Petite-Roselle in France, are supports of railroad tracks used in the pit head during around 50 to 60 years and then stored in outdoor unsheltered conditions, displayed in Figure 1a. These samples have a relative homogeneous thickness of corrosion layer of around 100 µm without traces of residual soil or coal. They were cut in small pieces of 1*1 cm^2 and carefully embedded in epoxy resin to mask the cut edges for electrochemical measurements, according to the scheme in Figure 1b. Then, the prepared samples were used as working electrode.

For metallographic observations and analysis, the metallographic cross-sections were polished with successive SiC emery papers up to 2400 under absolute ethanol, then with different diamond pastes without water. Samples were finally rinsed with ethanol and dried with hot air (around 40 °C).

The chemical analysis of the CL was realized by micro-Raman spectroscopy measurements performed on the metallographic cross section (Renishaw inVia reflex micro-Raman spectroscopy). Both the incident and the scattered lights are collected through a Leica microscope. Raman excitation was provided by a frequency-doubled Nd:YAG laser operating at 532 nm with a power of about 0.1 mW and with a probe diameter of about 1 µm. All spectra were calibrated using the 520.5 cm^{-1} line of a silicon wafer.

For X-ray diffraction analysis (XRD), the corrosion layers were sampled by scraping the surface and were crushed in an agate mortar to be analyzed by a Philips XPert Pro diffractometer equipped with copper anticathode ($\lambda_{k\alpha}$ = 1.5418 Å). Surface observations of the CL were carried out by Field Emission Scanning Electron Microscopy (FE-SEM JEOL J7600F), in backscattering electron (BSE) or secondary electron (SE) detection modes.

The reference corrosive medium in electrochemical experiments was the ASTM D1384-87 solution (noted ASTM [26]) with the following composition: 148 mg l^{-1} Na_2SO_4, 138 mg l^{-1} $NaHCO_3$ and 165 mg l^{-1} NaCl, at pH=8.3. Sodium decanoate solution $CH_3(CH_2)_8COONa$ noted NaC_{10} was obtained through the neutralisation of decanoic acid (from Aldrich) by sodium hydroxide solution until pH=8. Then, sodium decanoate or catechin (from Aldrich) were mixing with ASTM water at a desired concentration at pH=8 for the electrochemical measurements. Decanoic acid solution, $CH_3(CH_2)_8COOH$ noted HC_{10}, was just prepared by mixing decanoic acid and deionized water at natural pH = 4.5.

The electrochemical tests were performed, in aerated conditions, with a three-electrode electrochemical cell, connected to an EGG PAR 273A potentiostat and a frequency response

analyzer (Solartron FRA 1255), driven by a computer. In this configuration, the working electrode surface is horizontal, facing the Pt-grid counter electrode. The reference electrode was a KCl-saturated calomel electrode (Hg_2Cl_2/Hg, E = +0.242 V/SHE) and all the working electrode potentials were given versus this reference. Electrochemical impedance spectra were recorded at open-circuit potential (or corrosion potential) between 10^6 and 10^{-3} Hz with a 50 mV amplitude and 10 points per frequency decade, after a minimum of 30 min of immersion at open-circuit potential. The voltage amplitude was chosen in order to increase the signal/noise ratio, especially at low frequency, without changing the overall state of the system, by verifying the symmetry of the Lissajous plot (AC current versus AC potential).

Carbon pastes were prepared by mixing at 60 °C: 10 wt% of studied compound with 50 wt% of graphite powder and 40 wt% of paraffin wax as inert binder (in a liquid state). The liquid paste was inserted in a Plexiglas tube in contact with a Pt-wire. Then after cooling, the carbon paste surface was carefully polished with SiC emery paper. Voltammetric measurements with the carbon paste were carried out at 10 mV s^{-1} in Na_2SO_4 0.1 M support electrolyte (pH=7).

Goethite was provided from Alfa Aesar. Lepidocrocite and ferrihydrite were synthesised at 25 °C, following a procedure drawn from Cornell et al. [27], and analysed by XRD.

3. Results and interpretations

3.1 Analysis of thick corrosion layer (CL)

After metallographic etching with Nital reagent (5%vol HNO_3 in ethanol), the iron alloy of the railroad tracks reveals some zones of ferrite with ferrito-pearlitic structure with the presence of inclusions (Figure 1c). EDX analysis shows that carbon and phosphorous content is respectively inferior to 1 wt% and 0.1 wt%.

Concerning the composition of the corrosion layer (CL), X-ray diffraction pattern exhibit the presence of goethite, lepidocrocite and maghemite or magnetite, as often analyzed on this

kind of aged CL (Figure 2a) [8]. More precisely, microRaman spectroscopy allows distinguishing two distinct layers at the microscopic scale, as displayed in Figure 3 [28]:

- An internal layer, close to the metal, is mainly formed with goethite, characterized by the Raman peak at 380 cm^{-1} with areas of ferrihydrite and maghemite, identified by the peak at 700 cm^{-1} which is a very low-crystallized phase [29, 30]. This layer is relatively compact, particularly in the neighboring of the metal/oxide interface, and is sometimes called “black layer”.
- An external layer is very cracked and porous, and mainly composed by lepidocrocite, identified by the Raman band at 250 cm^{-1} [28, 30].

3.2 EIS measurements

In the ASTM corrosive electrolyte without corrosion inhibitor (containing chloride, sulfate, hydrogenocarbonate at pH=8.3), the corrosion potential of the metal/CL system rapidly reaches a stable value by decreasing from -370 mV to -400 mV after 50 h of immersion according to Figure 4. During the immersion, the electrochemical impedance spectra exhibit qualitatively the same features with immersion time (Figure 5). So, the CL rapidly reaches a steady state in this electrolyte.

These impedance spectra can be described with three main relaxation phenomena:

- At high frequency (between 10^5 and 10^4 Hz), the first capacitive loop is assigned to a charge transfer phenomenon, characterized by a very low capacitance value. By considering a resistance value around 1000 Ω cm^2 and a characteristic frequency (fc) around 5 10^4 Hz, the capacitance value can be estimated between 10^{-7} to 10^{-8} $F.cm^{-2}$ ($fc = (2\pi RC)^{-1}$). This value is lower than a usual double layer capacitance of a metal and could be attributed to the capacitance of a dielectric oxide film in contact with metal [11].

- At medium frequency (around 10^3 to 10^2 Hz), a second relaxation time can be distinguished, characterized by a very depressed capacitive loop on the Nyquist diagram, and can be assigned to the impedance of conductive porous electrode which could be explained by the theory of de Levie [31].
- At low frequency (below 1 Hz), a third time constant is clearly assigned to diffusion phenomenon in the electrolyte inside the large pores of the external CL. In the Nyquist representation, the impedance data show an angle of about 30° with the real axis, which suggest a Warburg-like component or an impedance in a semi-infinite porous medium [11, 12].

Nevertheless, as simulated in the theoretical work of S.J. Cooper et al. on the diffusion impedance in porous media, a clear assignment of the phenomenon at medium and low frequency is difficult because different relaxation times can appear in function of conductivity, microstructure and geometry of pores in this kind of aged corrosion layer [32]. Despite the fact that the thickness of CL is important, the overall impedance modulus without inhibitor does not exceed 10000 Ω cm^2 at low frequency after 48 h of immersion in ASTM water. According microstructural analysis and EIS measurements, a comprehensive structural model of this metal/CL system can be proposed in Figure 6a.

With addition of 10^{-2} M of sodium decanoate in ASTM water, the corrosion potential of the electrochemical system is sharply increased in the first hours of immersion, around 0 V, and stabilize around -100 mV after 20 h of immersion. This result reveals that decanoate ions have mainly an inhibiting action on the anodic reactions of the metal/CL system (Figure 4). In contrary, the addition of catechin has a very poor effect on the corrosion potential of the system. In fact, after some hours of immersion, the potential reach a value similar to the one measured without inhibitor.

After 24 hours of immersion, the measurements of impedance spectra with and without corrosion inhibitors are displayed and compared on Figure 7. Globally, the impedance spectra have the same features and can be interpreted with the same three relaxation phenomena detailed for the spectra without inhibitor in Figure 5.

At high frequency (between 10^4 and 10^5 Hz), the NaC_{10} addition slightly modifies the impedance modulus, from approximately 1000 to 2000 Ω cm^2, which indicates that decanoate ion has a weak effect on the layer at the metal interface.

Nevertheless, the presence of decanoate ions significantly increases the impedance modulus of the relaxation phenomenon at medium and particularly at low frequency. Indeed the impedance modulus at low frequency (below 1 Hz) is approximatively multiplied by a 3 to 4 factor with decanoate ions, which means that its addition decreases the diffusion of ionic species such as iron cations and hydroxyl ions in the pores network.

X-ray diffraction analysis of the metal/CL system immersed in 10^{-2} M NaC_{10} during 5 days shows the characteristic diffraction (001) and (002) peak at low angle of iron decanoate, which can be noted $Fe(C_{10})_3$ in Figure 2c, according to previous study on iron carboxylate compounds by X-ray absorption spectroscopy at the iron K-edge and XRD [33]. So, at neutral pH in ASTM corrosive water, decanoate anions are able to form insoluble iron decanoate in the CL and to block the diffusion of iron cations in the layer (figure 2b). However, the chemical conversion of FeOOH compounds into iron decanoate formation seems to be limited in this neutral pH in ASTM water.

Regarding the catechin addition, the presence of catechin compound in ASTM water has a weak influence on the overall impedance modulus of the metal/CL system. At high frequency, the impedance modulus increases from 1000 Ω cm^2 without inhibitor to 2000 Ω cm^2 with catechin (at 5 10^4 Hz), which indicates a slight increase of the resistance at the metal interface with catechin (Figure 7a).

Thus, according to EIS analysis and surface analysis, decanoate species are able to increase the impedance modulus of the metal/CL system by forming iron decanoate inside the corrosion layer. In the following sections, a treatment in acid media (at pH=4.5) with a decanoic acid (HC_{10}) solution will be used to increase the chemical conversion of FeOOH compounds into iron decanoate. Then, the corrosion behavior of HC_{10}-treated metal/CL system was evaluated by EIS in ASTM corrosive water.

3.3 Electrochemical activity of iron oxyhydroxides in presence of corrosion inhibitor

In order to evaluate the influence of the HC_{10} conversion treatment on FeOOH compounds, the electrochemical activity of the main iron oxyhydroxide phases in the CL was studied in carbon paste electrode in neutral support electrolyte. Figure 8 gathers the voltammograms of lepidocrocite, goethite and ferrihydrite without inhibitor, which shows all a broad oxidation current peak around -0.3 to -0.2 V, and a reduction current peak around -1 V. However, the maximum oxidation and reduction current are very different in these two potential domains in function of FeOOH phases. According to most authors [34, 35], these two peaks are due to an electronic exchange between Fe(III) and Fe(II) species, and the broadness of the peaks likely corresponds to several electrochemical processes, which are not yet well-known. Nevertheless, the experimental studies and theoretical calculation of Charlet et al. show that the FeOOH/Fe^{2+} redox couple have a very low equilibrium potential, around -0.5 to -0.6 V /SCE, compared to classical equilibrium potential of Fe(III)/Fe(II) redox couple [36]. So, these peaks can correspond to the overall redox equation between FeOOH solid phases and aqueous or adsorbed Fe^{2+} cations:

$FeOOH_{(s)} + e^- + 3H^+ \rightarrow Fe^{2+}_{(aq)} + 2H_2O$.

So, the maximum reduction peak current at -1 V is meaningful to evaluate the electrochemical reactivity of each phase. In this case, the most reactive phase, with the highest reduction peak,

is ferrihydrite, then lepidocrocite, and the more inert phase is goethite, as already observed by Anthony et al. with another coulometric method [37].

The most abundant phase in the external part of the CL, lepidocrocite (Figure 9), has been treated by simple immersion in corrosion inhibitor, decanoic acid solution and catechin solution at pH 4.5 during 5 days.

For the HC_{10} treatment, the presence of the diffraction peak at low angle in Figure 10 is characteristic of the formation of crystallized iron carboxylate $Fe(C_{10})_3$, shown in Figure 10d. HC_{10} treated-lepidocrocite is partially transformed in iron carboxylate during this immersion treatment (Figure 10b, c) compared to non-treated lepidocrocite in Figure 10a. The voltammetric measurement in CPE of the HC_{10}-treated lepidocrocite shows a sharp decrease of the reduction peak current, which reveals that the electrochemical activity of lepicocrocite is almost completely inhibited by the immersion treatment in HC_{10} solution (Figure 9a).

Concerning the catechin treatment, the immersion of lepidocrocite in 0.1 M catechin solution does not modify the X-ray diffractogram and Raman spectra of the FeOOH phase, although the lepidocrocite powder becomes blue-black color (data not shown). This observation indicates that the reaction of lepidocrocite with catechin to form blue black iron catecholate complex only occurs on the grains surface of FeOOH. The low chemical conversion of FeOOH in blue-black color catecholate complex is well-corroborated with the low reduction of current peak of the catechin-treated lepidocrocite in CPE. Consequently, the electrochemical activity of FeOOH phase is poorly affected by the catechin treatment in these conditions.

Consequently, the immersion in acidic solution leads to an increase of iron(III) dissolution, then precipitation into iron decanoate in bulk or iron catecholoate, only on the grain surfaces, according to the schematic reactions [33, 37]:

$Fe(III) + 3HC_{10} \rightarrow Fe(C_{10})_3 + 3H^+$

$Fe(III) + 3Cat \rightarrow Fe(Cat)_3$ (where cat represents catecholate organic function).

3.3 Inhibiting treatment of CL

The inhibiting treatment in HC_{10} decanoic acid solution was then performed in the overall metal/CL system. After treatment, SEM observations in BSE mode (Figure 11) display that the HC_{10}- treated surface is partially covered by thick iron carboxylate deposit. The SEM zoom image in SE mode confirms the crystallization of iron carboxylate platelets. In fact, at a micrometer scale, the iron carboxylate coating is not homogeneous because the composition of the CL and its reactivity are not homogeneous. Nevertheless, the HC_{10}-treated corrosion layers show macroscopically no change of colors and aspects after 5 days of treatment.

The corrosion potential and impedance spectra of treated system were regularly recorded during 30 days in ASTM corrosive water. As can be seen in Figure 12, the corrosion potential of HC_{10}-treated metal/CL system remains approximately 400 mV higher than the one of non-treated metal/CL system in the ASTM corrosive water. It is noteworthy that the corrosion potential remains very stable even during long immersion time for the non-treated and treated system.

Throughout the immersion in the corrosive water, the EIS spectra of the non-treated and HC_{10}-treated sample have the same features and can be also described with three main relaxation phenomena (Figure 13).

In the first hours of immersion (at 48 hours), the impedance spectra of HC_{10}-treated sample, displayed on Figure 13, show an overall increase impedance modulus in all the frequency range. Particularly, the impedance modulus assigned to the diffusion phenomena at low frequency (below 1 Hz) in the external layer is multiplied by a ten factor (Figure 13a). Even after a long immersion time (at 480 h), the impedance modulus values of the HC_{10}-treated CL

remain high which underlines the good stability of the HC_{10}-treated corrosion layer all over the immersion time in this corrosive media (Figure 13b).

Consequently, the treatment of metal/CL system in a 0.1 M HC_{10} solution at pH 4.5 clearly induces the formation of iron decanoate by chemical conversion, which covers the surface of FeOOH phase and seals some pores and some areas.

A schematic structural model of the HC_{10}-treated metal/CL system is proposed in Figure 6b. Even though the chemical conversion of corrosion layer is not homogeneous as shown by SEM observations, the impedance measurements show that this conversion layer increases the overall impedance of the system by inhibiting the dissolution phenomenon of FeOOH phases and reducing the diffusion phenomenon through the pores network.

4. Conclusion

Through the results of this study, the mechanism of corrosion inhibition in metal/CL system is mainly based on the blocking of the dissolution of FeOOH-type phase and hindering of the diffusion of ionic species inside the pore network of CL. Indeed, addition of decanoate anions in corrosive medium or a decanoic acid treatment of CL allow one to increase the impedance of CL layer and limit the diffusion inside the layer. The inhibition mechanism is a chemical conversion of the reactive iron oxyhydroxide, as lepidocrocite, into iron carboxylates (or iron soaps). This iron soap inhibits the electrochemical activity of FeOOH-type phases and blocks the dissolution of FeOOH, as demonstrated with CPE experiments.

Regarding the catechin, although many rust compounds are transformed in surface into blue-black colored compounds, which are appreciated by curators, the catechin has a slight influence on the electrochemical activity of FeOOH type phases .

From an electrochemical point of view, even if the different relaxation phenomenon are difficult to identify in details in the complex metal/CL systems on iron, electrochemical

impedance measurements are very relevant and useful to evaluate the mechanism of corrosion inhibition on such complex electrochemical system on iron-based alloys.

References

[1] J Alfrey, T. Putnam “The Industrial heritage: Managing resources and uses”, Taylor and Francis, London (GB), 2003

[2] U.R. Evans, C.A.J. Taylor, Mechanism of Atmospheric Rusting. Corrosion Science, 12(3) (1972) 227-246.

[3] M. Stratmann, K. Bohnenkamp, H.J. Engell, An electrochemical study of phase transitions in rust layers. Corrosion Science, 23(9) (1983) 969-985.

[4] M. Stratmann, The atmospheric corrosion of iron - a discussion of the physico-chemical fundamentals of this omnipresent corrosion process. Invited review, Berichte der Bunsen-Gesellschaft, 94(6) 1990 626-639

[5] M. Stratmann, J. Müller, The mechanism of the oxygen reduction on rust-covered metal substrates. Corrosion Science 36(2) 1994 327-359.

[6] J. Monnier, E. Burger, P. Berger, D. Neff, I. Guillot, P. Dillmann, Localisation of oxygen reduction sites in the case of iron long term atmospheric corrosion, Corrosion Science 53(8) 2011 2468-2473

[7] D. Neff, P. Dillmann, L. Bellot-Gurlet, G. Beranger, Corrosion of iron archaeological artefacts in soil: characterisation of the corrosion system, Corrosion Science 47(2) 2005 515-535

[8] M. Bouchar, P. Dillmann, D. Neff, New Insights in the Long-Term Atmospheric Corrosion Mechanisms of Low Alloy Steel Reinforcements of Cultural Heritage Buildings. Materials (Basel) (2017) 10

[9] M.C. Bernard, S. Joiret, Understanding corrosion of ancient metals for the conservation of cultural heritage, Electrochimica Acta 54 (2009) 5199–5205

[10] D. Neff, L. Bellot-Gurlet, P. Dillmann, S. Reguer, L. Legrand, Raman imaging of ancient rust scales on archaeological iron artefacts for long-term atmospheric corrosion mechanisms study, Journal of Raman spectroscopy 37(10) 2006 1228-1237

[11] I. Frateur, C. Deslouis, L. Kiene, Y. Levi, B. Tribollet, Free chlorine consumption induced by cast iron corrosion in drinking water distribution systems, Water Research 33(8) (1999) 1781–1790.

[12] O.E. Barcia, E. D'Elia, I. Frateur, O.R. Mattos, N. Pébère, B. Tribollet, Application of the impedance model of de Levie for the characterization of porous electrodes, ElectrochimicaActa 47 (2002) 2109–2116.

[13] R. de Levie, in: P. Delahay, C.W. Tobias (Eds.), Advances in Electrochemistry and Electrochemical Engineering - Vol. 6, Interscience, New York, 1967, p. 329.

[14] M. Sancy, Y. Gourbeyre, E.M.M. Sutter, B. Tribollet Mechanism of corrosion of cast iron covered by aged corrosion products: Application of electrochemical impedance spectrometry, Corrosion Science 52 (2010) 1222–1227

[15] V. Otieno-Alego, G. Neath, D. Hallam, D. Creagh, Metals 98, (Eds) James and James Ltd., (1998) 309-314

[16] J. Gust, J. Bobrowicz, Sealing and Anti-Corrosive Action of Tannin Rust Converters, Corrosion 49(1) 1993 24-30

[17] O. R. Pardini, J. I. Amalvy, A. R. Di Sarli, R. Romagnoli, V. F. Vetere, Formulation and testing of a waterborne primer containing chestnut tannin, Journal of Coatings Technology 73(913) (2001) 13 99–106

[18] A. A. Rahim, M. J. Kassim, E. Rocca, J. Steinmetz, Mangrove (Rhizophora apiculata) tannins: an eco-friendly rust converter, Corrosion Engineering Science and Technology 46(4) (2011) 425-431

[19] A. A.Rahim, E. Rocca, J. Steinmetz, M. Jain Kassim, Inhibitive action of mangrove tannins and phosphoric acid on pre-rusted steel via electrochemical methods, Corrosion Science (2008) 50(6) 1546-1550

[20] C. Georges, E. Rocca, P. Steinmetz, Synergistic effect of tolutriazol and sodium carboxylates on zinc corrosion in atmospheric conditions, Electrochimica acta (2008) 53 4839-4845

[21] E. Rocca, G. Bertrand, C.Rapin, J.C. Labrune, Inhibition of copper aqueous corrosion by non-toxic linear sodium heptanoate : mechanism and ECAFM study, Journal of Electroanalytical Chemistry 503 (2001) 133-140.

[22] E. Rocca, J. Steinmetz, Inhibition of lead corrosion with saturated linear aliphatic chain monocarboxylates of sodium, Corrosion Science 43 (2001) 891-902.

[23] E. Rocca, C. Rapin, F. Mirambet, Inhibition treatment of the corrosion of lead artefacts in atmospheric conditions and by acetic acid vapour : use of sodium decanoate, Corrosion Science 46 (2003) 653-665

[24] A Mesbah, C. Juers, F. Lacouture, S. Mathieu, E. Rocca, M. Francois, J. Steinmetz, Inhibitors for magnesium corrosion: Metal organic frameworks, Solid State Sciences, 9 (2007) 322-328

[25] A. A.Rahim, E. Rocca, J.Steinmetz, M. J. Kassim, R. Adnan, M. Sani Ibrahim, Mangrove tannins and their flavanoid monomers as alternative steel corrosion inhibitors in acidic medium, Corrosion Science 49(2) (2007) 402-417

[26] ASTM Standard D 1384, in: Standard test method for corrosion test engine coolants in glassware, ASTM, West Conshohocken, PA, 1988

[27] R. Cornell, U. Schwertmann, The iron oxides - Structure, Properties, Occurrences and Uses 2nd ed., Wiley-VCH, Weinheim (2003).

[28] D. Neff, L. Bellot-Gurlet, P. Dillmann, S. Reguer, L. Legrand, Raman imaging of ancient rust scales on archaeological iron artefacts for long-term atmospheric corrosion mechanisms study, Journal of Raman spectroscopy 37(10) 2006 1228-1237

[29] L. Mazzetti, P.J. Thistlethwaite, Raman spectra and thermal transformations of ferrihydrite and schwertmannite, Journal of Raman Spectroscopy 33(2) (2002) 104-111

[30] D.L.A. De Faria, S.V. Silva, M.T. de Oliveira, Raman microspectroscopy of some iron oxides and oxyhydroxides, Journal of Raman Spectroscopy 28 (1997) 873–878.

[31] R. de Levie, Advances in Electrochemistry and Electrochemical Engineering 6 (1967) 329

[32] S. J. Cooper,, A. Bertei, D. P. Finegan, N. P. Brandon, Simulated impedance of diffusion in porous media, Electrochimica Acta 251 (2017) 681–689

[33] F. Mirambet, S. Reguer, E. Rocca, A complementary set of electrochemical and X-ray synchrotron techniques to determine the passivation mechanism of iron treated in a new corrosion inhibitor solution specifically developed for the preservation of metallic artefacts, Applied Physics A-Materials Science and Processing 99(2) (2010) 341-349

[34] E.R. Vago, E.J. Clavo, Electrocatalysis of oxygen reduction at iron oxide (Fe_3O_4) electrodes in alkaline solutions, Journal of Electroanalytical Chemistry 339 (1992) 41-67

[35] P.D. Allen, N.A. Hampson, J.F. Tyson, G.J. Bignold, The electrodissolution of magnetite: Part I. The electrochemistry of Fe3O4/C discs-potentiodynamic experiments, Journal of Electroanalytical Chemistry and interfacial chemistry, 99(3) (1979) 299-309.

[36] L. Charlet, E. Silvestre, E. Liger, N-compound reduction and actinide immobilization in surficial fluids by Fe(II): the surface ≡FeIIIOFeIIOH° species, as major reductant, Chemical Geology 151 (1998) 85-93.

[37] H. Antony, S. Perrin, P. Dillmann, L. Legrand, A. Chausse, Electrochemical study of indoor atmospheric corrosion layers formed on ancient iron artefacts, Electrochimica Acta 52(27) (2007) 7754-7759

[38] D. Veys-Renaux, S. Reguer, L. Bellot-Gurlet, F. Mirambet, E. Rocca, Conversion of steel by polyphenolic model molecules: corrosion inhibition mechanism by rutin, esculin, Corrosion Science 136 (2018) 1-8.

a)

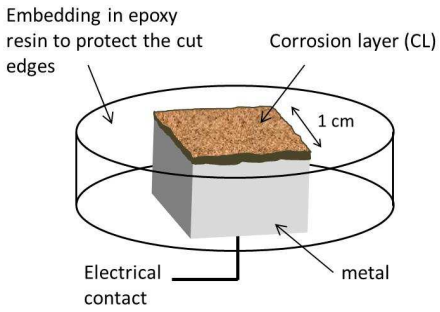

b)

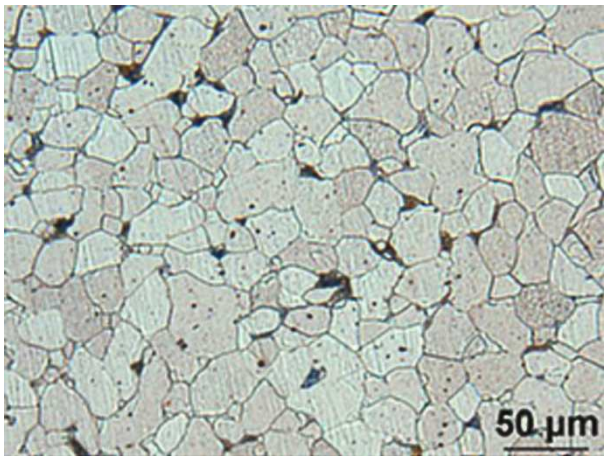

c)

Figure 1: (a) Macroscopic photo of corroded railroad track (The black underlined area are sampling zones) , b) Schematic representation of prepared working electrode with the corroded railroad track

(c) Optical micrograph of steel of corroded railroad tracks.

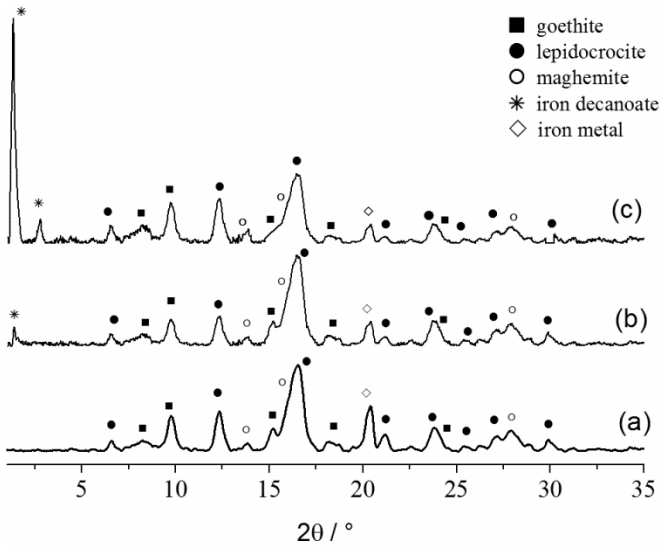

Figure 2: X-ray diffractograms of corrosion layer without inhibition treatments (a), after 5 days of immersion in NaC_{10} 10^{-2} M solution (b), after 5 days of immersion in 0.1 M HC_{10} solution (c)

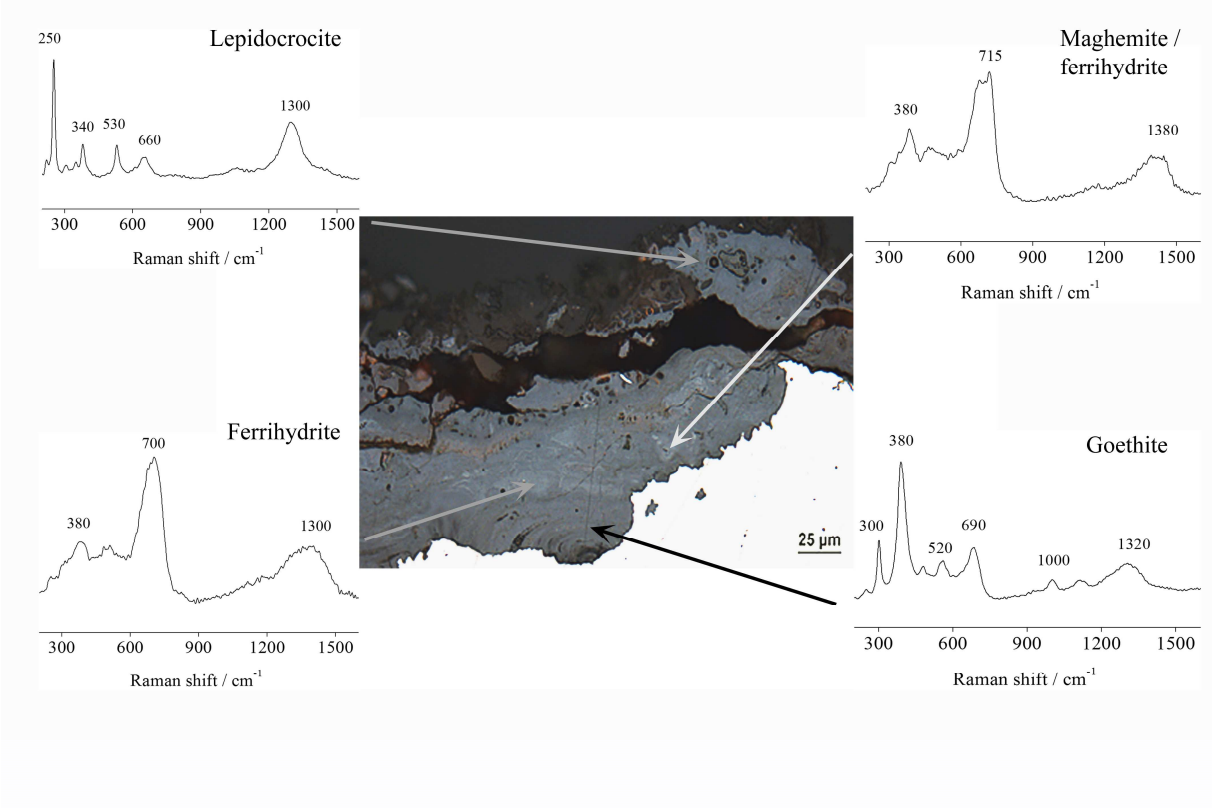

Figure 3: Optical metallographic cross section of the metal/corrosion layer (CL) with mico-Raman spectra of the different zones of CL.

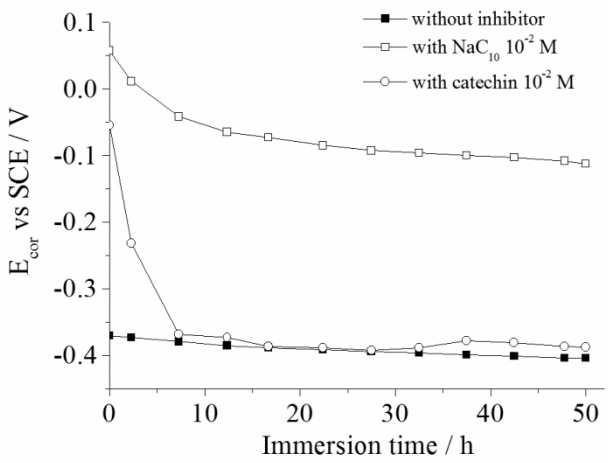

Figure 4: Corrosion potential measurements of "metal/CL" system versus immersion time in ASTM corrosive water without or with corrosion inhibitors.

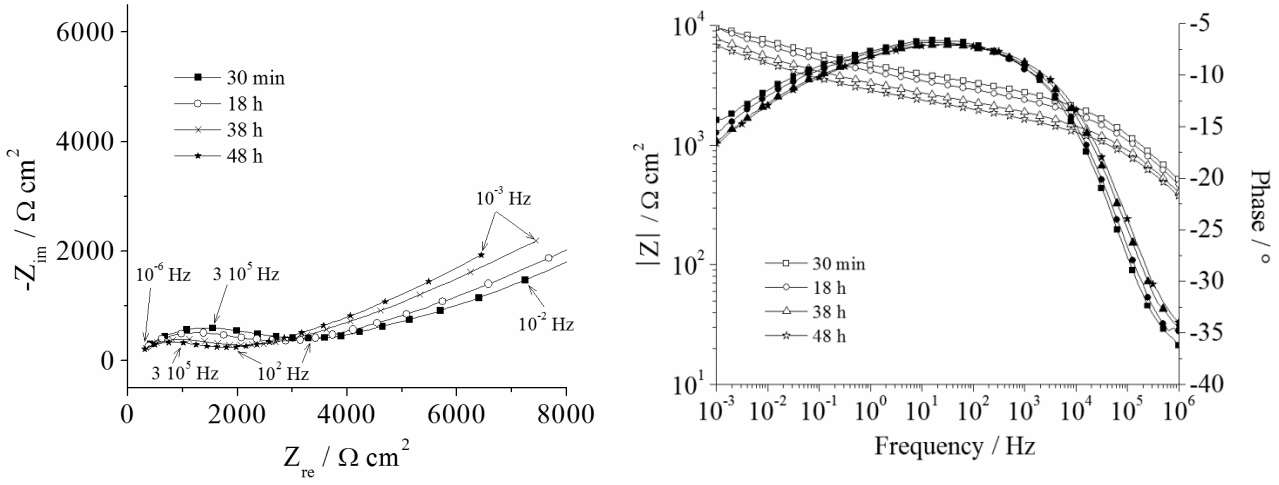

a) b)

Figure 5: Impedance diagram of "metal/CL" system in ASTM corrosive water at different immersion time in (a) Nyquist representation and (b) Bode representation.

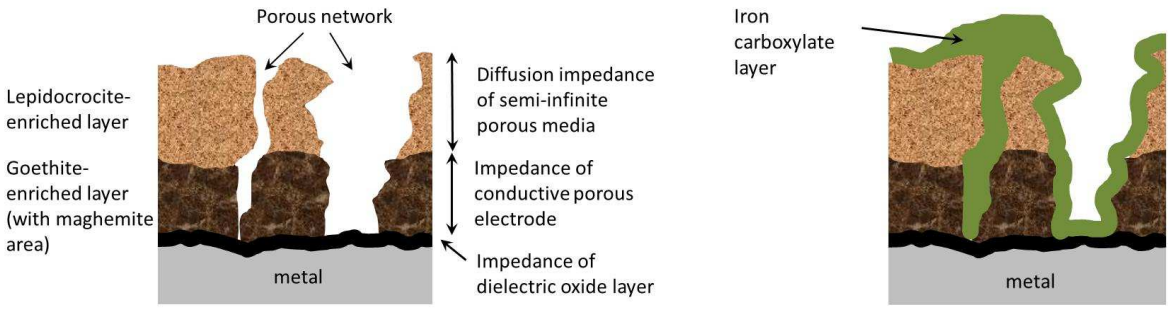

a) b)

Figure 6: (a) Schematic structural model of the "metal/CL" system, (b) HC_{10}-treated structure of "metal/CL" system

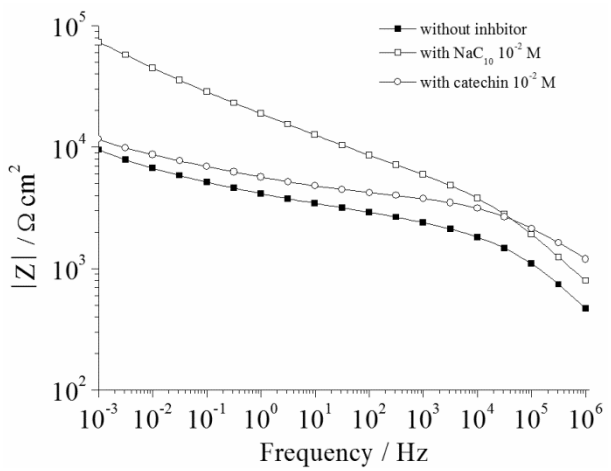

a)

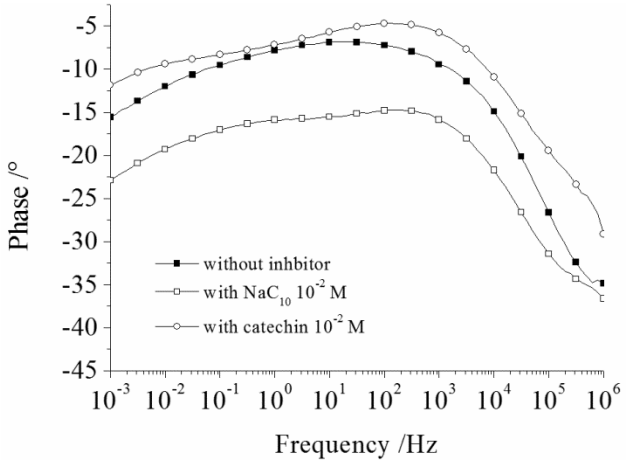

b)

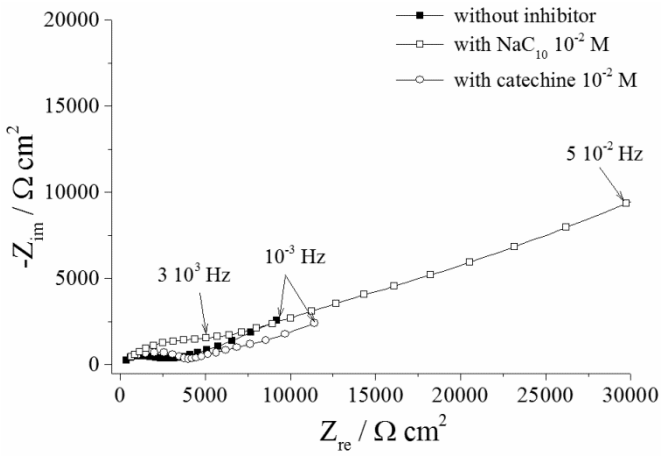

c)

Figure 7: Impedance diagram of “metal/CL” system in ASTM corrosive water without and with corrosion inhibitors after 24 hours of immersion. (a, b) Bode representation, (c) Nyquist representation.

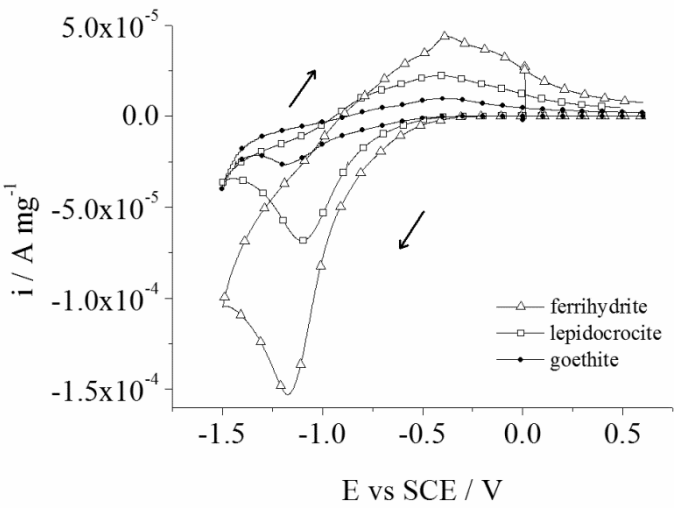

Figure 8: Voltammogram of different iron oxyhydroxide phase in CPE in Na_2SO_4 0.1 M electrolyte

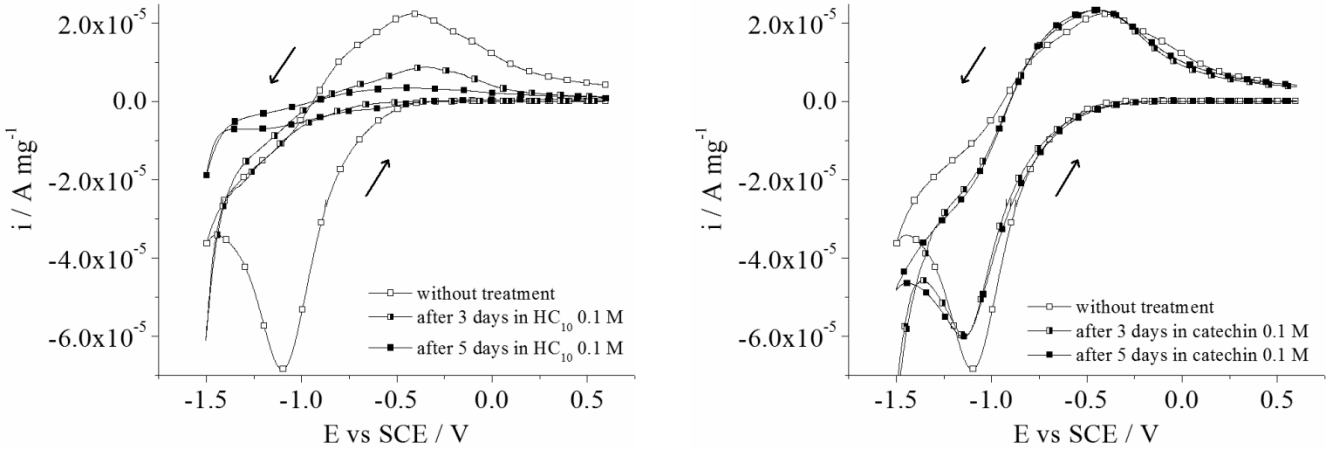

a) b)

Figure 9 : Voltammogram of lepidocrocite in CPE in Na_2SO_4 0.1 M electrolyte without treatment and after immersion in (a) HC_{10} solution and (b) catechin solution

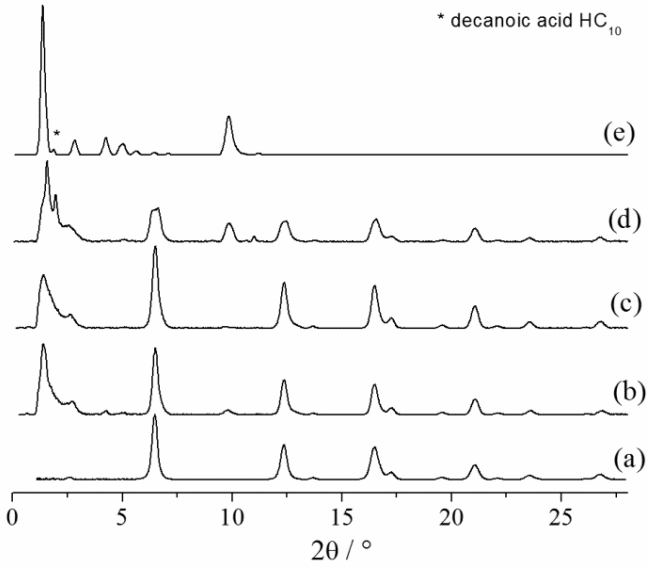

Figure 10 : X-ray diffractogram of lepidocrocite without treatment (a), lepidocrocite treatedwith HC_{10} solution for (b) 1 day, (c) 3 days, (d) 5 days, and (e) synthesized iron decanoate from [36].

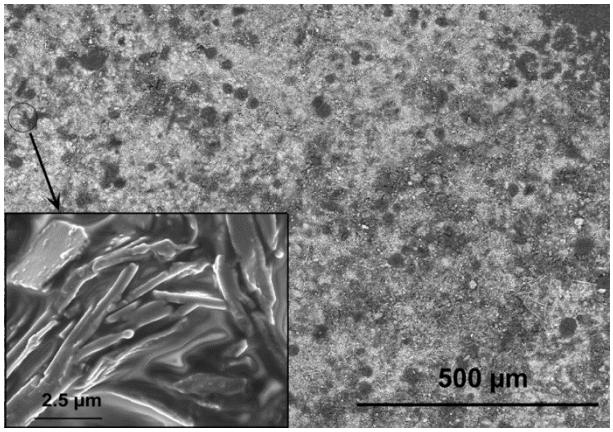

Figure 11: SEM observation of surface of CL after HC_{10}-based conversion treatment (5 days in HC_{10} 0.1 M) in BSE mode and zoom of iron carboxylate deposit in SE mode

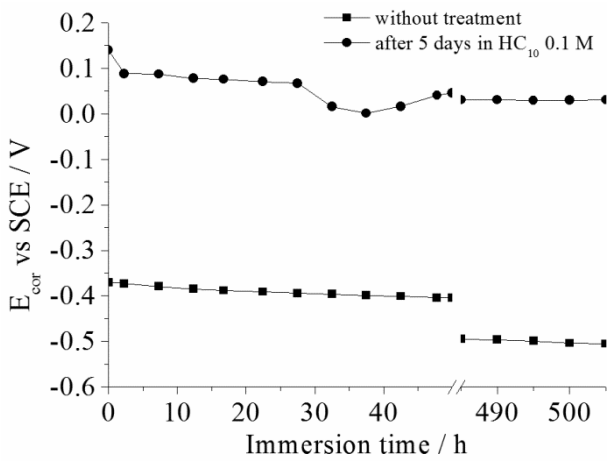

Figure 12: Corrosion potential measurements of "metal/CL" system versus immersion time in ASTM corrosive water without treatment and after HC_{10}-based conversion treatment.

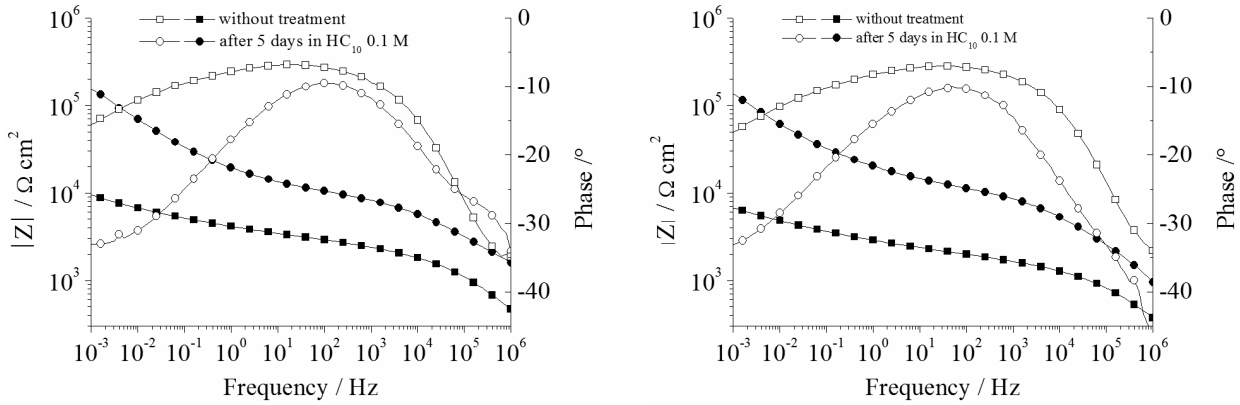

a) b)

Figure 13: Impedance diagram of "metal/CL" system without and with HC_{10}-based conversion treatment (5 days in HC_{10} 0.1 M) after (a) 48 h and (b) 480 h of immersion in ASTM corrosive water.